JOURNAL OF APPLIED POLYMER SCIENCE VOL. 17, PP. 2369-2393 (1973)

# Studies of Converging Flows of Viscoelastic Polymeric Melts. III. Stress and Velocity Distributions in the Entrance Region of a Tapered Slit Die

CHANG DAE HAN and LEONARD H. DREXLER,
*Department of Chemical Engineering, Polytechnic Institute of Brooklyn, Brooklyn, New York 11201*

## Synopsis

An experimental and theoretical study has been carried out, as a continuation of our previous investigation, to better understand the problems associated with converging flows of viscoelastic polymeric melts. In the present study, measurements were taken of both stresses and velocities in the converging velocity field of polymeric melts flowing into a tapered slit die, stresses by means of the flow birefringence technique and velocities by means of streak photography. The material used was polystyrene. A theoretical analysis was also made of converging flow, using a modified second-order fluid model which assumes that all three material functions depend on the second invariant of the rate of deformation. Numerical solutions were obtained of the equations of motion, which give predicted velocity profiles in reasonable agreement with the measured velocity profiles. A comparison was also made of the experimentally determined stress distributions with the theoretically predicted ones.

## INTRODUCTION

A better understanding of converging flow of viscoelastic polymeric melts is very important from both the practical and theoretical points of view. From a practical point of view, it will help provide valuable information on the design of extrusion dies of industrial importance (e.g., spinnerettes and film dies) and develop useful correlations between the rheological properties of the molten polymers and the processing variables affecting pressure drop and the extent of extrudate swell. From a theoretical point of view, converging flow, representing a nonviscometric flow, will provide an opportunity for testing the usefulness of various constitutive equations in other than viscometric flow.

In the present paper, we shall first present our recent measurements of stresses and velocities in a viscoelastic polymeric melt flowing through a tapered slit die, having a half-angle of 30 degrees at the die entrance. The flow birefringence technique was used to measure stress-birefringent patterns, and the technique of streak photography to measure the local veloci-



© 1973 by John Wiley & Sons, Inc.

ties of tracer particles suspended in polymer. The material used was polystyrene, and all measurements were taken at 200°C.

A theoretical analysis was also made of converging flow, using a modified second-order fluid model, which assumes that all three material functions depend on the second invariant of the rate of deformation. With some simplifying assumptions concerning the relationships between the material functions, the equations of motion were solved numerically in order to predict the velocity and stress profiles. A comparison was then made of these with the experimentally determined velocity and stress distributions.

## EXPERIMENTAL

The experimental apparatus used for the present study was essentially the same as that described in part I of this series,[1] except for the modification of a test cell. In the present study, one of the test cells, referred to as Cell #1 in part I of this series, was modified so that the slit die had an entrance angle of 60 degrees instead of a sharp-edged entrance.

In the present study, both the stress-birefringence patterns and local velocities were measured in the converging channel, the former by use of the polariscope following the experimental procedure as described in part I of this series,[1] and the latter by means of streak photography following the experimental procedure as described in part II of this series.[2]

The polymer used for the present study was a general-purpose polystyrene (Dow Chemical, Styron 686). This is the same material used in parts I and II of this series.

## RESULTS

### Stress-Birefringent Patterns and Streak Photographs

Figure 1 gives representative pictures of isochromatic fringe patterns, in which it is seen that, as expected, the order of fringes increases with flow rate. A few qualitative observations can be made in Figure 1. First, the isochromatic bands (black and white) are convex along the centerline in the direction of melt flow. This is quite different from the case where the same material flows into a sharp-edged entrance (see Fig. 5 in part I of this series). The convexity of isochromatic fringe patterns along the centerline indicates a much stronger accelerative flow in a converging channel than in a sharp-edged entrance die. Second, the fringe patterns emanate from the center of the plane at which the slit die section truly begins. This indicates that stress keeps increasing as a melt flows from the upstream section into the entrance of the die section where maximum stresses are achieved. Third, at a distance of about twice the slit thickness from the entrance, the isochromatic fringe patterns are seen to be parallel to the slit die wall, indicating that the stresses have become independent of longitudinal direction (i.e., flow direction). This observation is in conformity with the one described in part I of this series.[1]

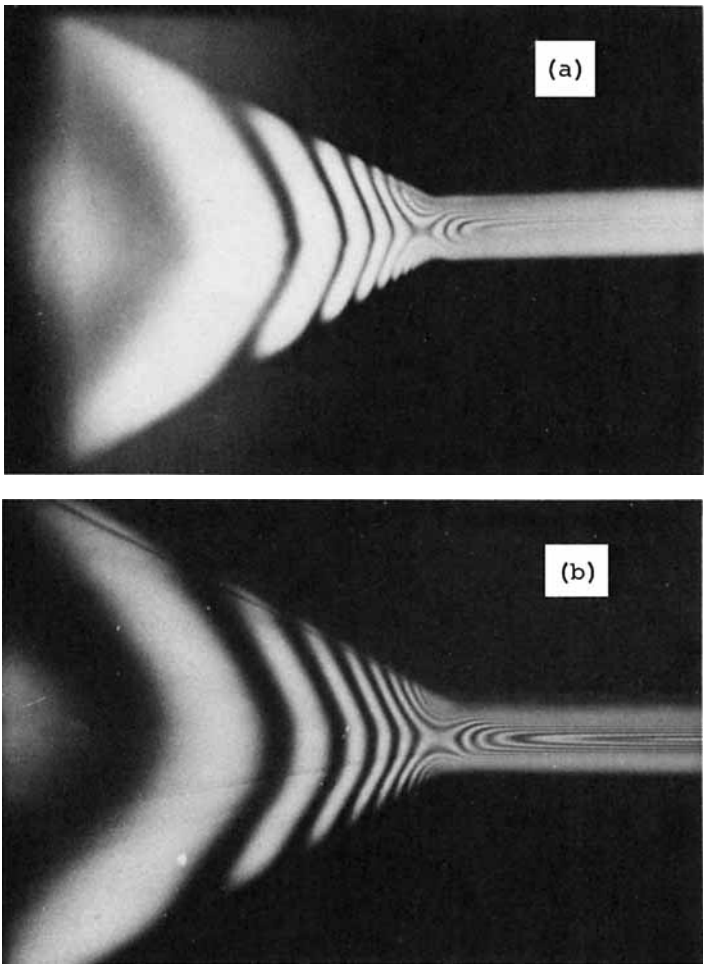


Fig. 1. Isochromatic fringe patterns of polystyrene melts at 200°C in a converging channel having a half-angle of 30 degrees: (a) $Q = 2.82$ cc/min; (b) $Q = 4.33$ cc/min.

Pictures of representative isoclinic fringe patterns are given in Figure 2 at two different isoclinic angles, 30 and 50 degrees. It is seen in these pictures that dark, broad bands emanate from somewhere near the slit die entrance. It should be noted that the complete elimination of isochromatic fringe patterns was not possible when isoclinic fringe patterns were being recorded when using a plane polariscope. This was mentioned in part I of this series. The importance of isoclinic fringe patterns to quantitatively determine the shear stress and normal stress differences has also been described in the previous paper.[1]

Figure 3 gives a representative streak photograph of tracer particles (copper powders of 70% 44 microns and 30 % 149 microns) suspended in a molten polystyrene flowing through a converging channel. Over 20 pic-

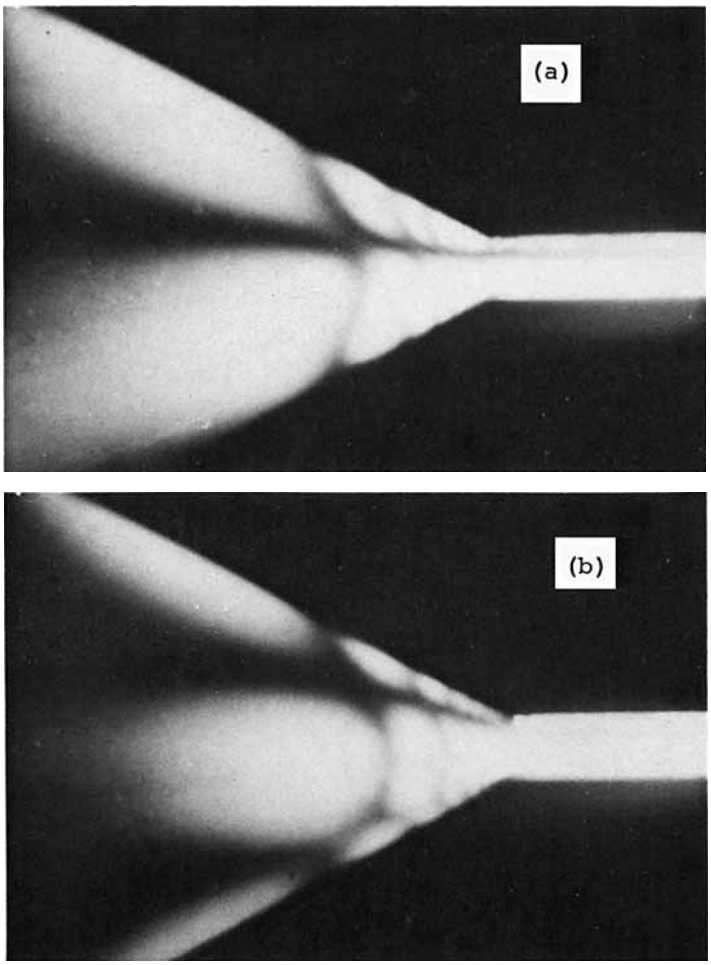


Fig. 2. Isoclinic fringe patterns of polystyrene melts at 200°C in a converging channel having a half-angle of 30 degrees: (a) isoclinic angle of 30 degrees; (b) isoclinic angle of 50 degrees.

tures were taken at a fixed flow rate. It is seen in this picture that streaklines at the centerline are longer than those away from the centerline, indicating that particles at the center travel faster than those away from the centerline. It is also seen that streaklines near the entrance of the slit die section are longer than those in the upstream.

It is appropriate at this point to discuss some important implications of the streak photograph shown in Figure 3. All the streaklines are oriented toward the die entrance, without showing any evidence of circulatory motion near the die entrance. This contradicts certain theoretical studies[3–5] reported in the literature, which dealt with the flow of viscoelastic fluids through a converging channel, bounded by two nonparallel planes.

Fig. 3. Streak photograph of polystyrene melts at 200°C in a converging channel having a half-angle of 30 degrees; $Q = 8.44$ cc/min.

In their analyses, these authors employed the perturbation technique, and they all concluded that the inclusion of second-order perturbation terms, which bring non-Newtonian effects, predicts velocity profiles having superposed secondary circulation patterns.

However, to the best of the present authors' knowledge, there has been no experimental evidence reported to support those theoretically predicted secondary circulation patterns in the flow of *polymer melts* through a converging channel. Certainly, both the stress-birefringent patterns and streak photographs reported in this study do not show such patterns. However, this is not surprising to us when considering the velocity of polymetric melts in terms of Reynolds number. Because of the exceedingly large values of viscosity of polymer melts, as compared to those of dilute polymeric solutions, the Reynolds number in polymer melt flow is usually very low, say below $10^{-2}$. It was certainly below $10^{-3}$ in the present experimental study. In other words, under the experimental conditions at which the flow is considered to be very slow, the visual detection of a noticeable circulatory motion may be very difficult to make, if not impossible.

## Stress and Velocity Distributions

Having recorded both the flow birefringence data (isochromatic and isoclinic fringe patterns) and velocity data (streak photographs), we were in a position to quantitatively determine profiles of stress and velocity. The analysis of experimental data was carried out using the schematic diagram of flow geometry given in Figure 4 and the procedures described in parts I and II of this series.

Figures 5 and 6 represent the shear stress and normal stress difference profiles, respectively, of polystyrene melts at 200°C, flowing through the

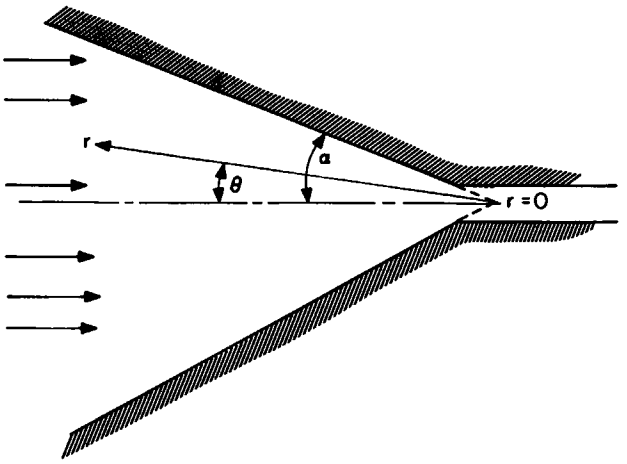


Fig. 4. Schematic of flow geometry.

tapered slit die having an entrance angle of 60 degrees (a half-angle of 30 degrees). The normal stress difference profiles are quite different from those for a sharp-edged die, as given in Figures 11 to 16 of part I of this series[1] on two accounts. One is that, in the tapered die (60 degrees entrance angle), the stresses emanate from the slit region, whereas in the sharp-edged die (180 degrees entrance angle) the stresses emanate from the corner of the slit. Another is that, in the tapered die, the stresses end

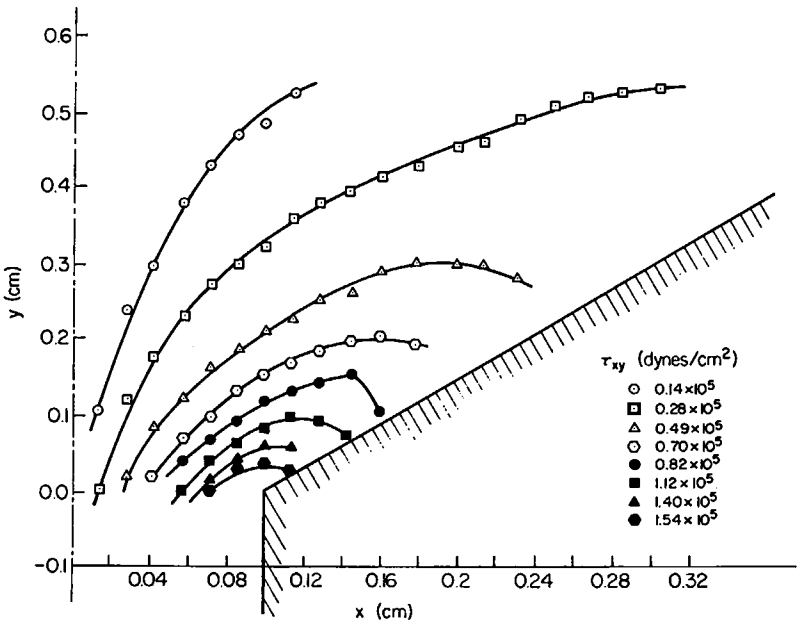


Fig. 5. Experimental shear stress profiles of polystyrene melts at 200°C; $Q$ = 5.36 cc/min.

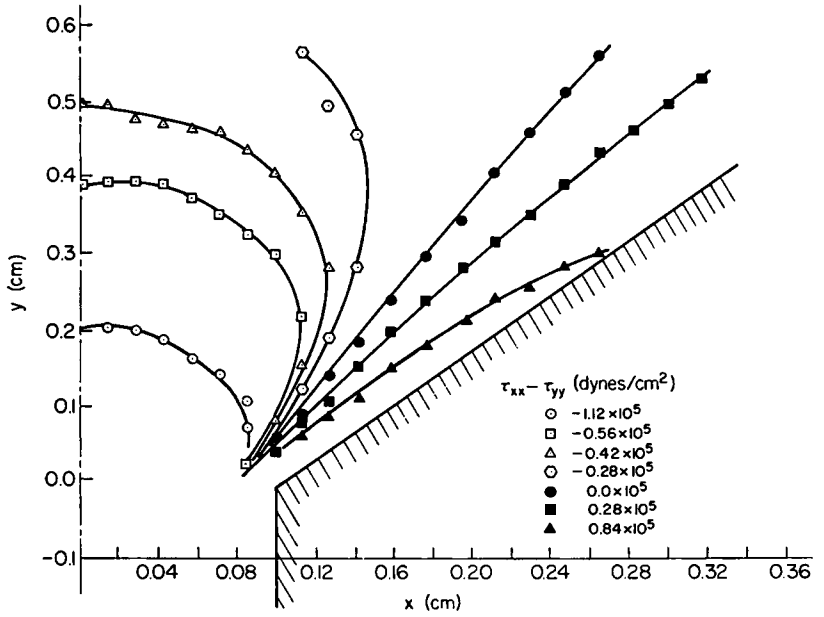


Fig. 6. Experimental normal stress difference profiles of polystyrene melts at 200°C; $Q$ = 5.36 cc/min.

at the wall of the wedge, whereas in the sharp-edged die the stresses form loops in the corners of the upstream reservoir. The differences are also evident when the shear stress profiles in the two cases (60 and 180 degrees entrance angles) are compared.

Figure 7 gives the velocity profiles at various radial positions from the vertex (see also Fig. 4). As noted in part II of this series,[2] a particular radial position in Figure 7 represents the distance measured along the streamlines of the system from its vertex. In Figure 7, the dotted lines represent the observed data, while the solid lines are the theoretically

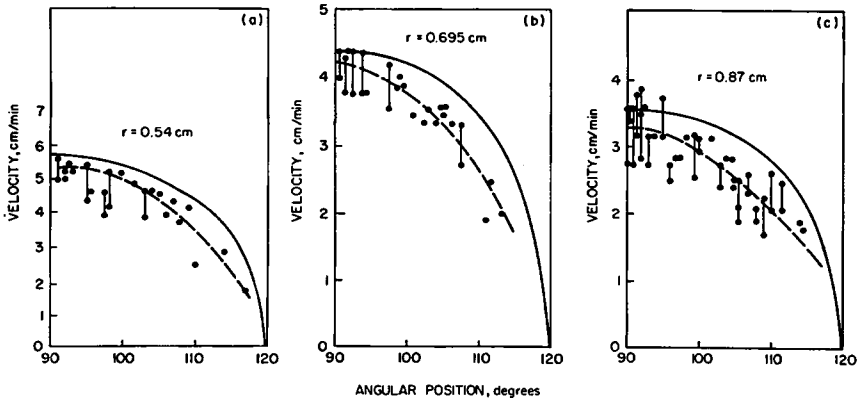


Fig. 7. Experimental velocity profiles of polystyrene melts at 200°C; $Q$ = 4.33 cc/min.

predicted velocity profiles obtained by solving the equations of motion with the use of a modified second-order constitutive equation. Details of the theoretical analysis carried out in the present study will be presented below.

## THEORETICAL ANALYSIS

Having experimentally determined both the stress and velocity distributions, we shall now give theoretical consideration to converging flows of viscoelastic polymeric melts.

For this, we shall consider the wedge flow, that is, the flow of a polymer melt flowing between two nonparallel planes which converge toward the entrance as schematically shown in Figure 4. For the wedge flow, streamlines will be assumed to be emanating radially from the point of intersection of the two nonparallel planes. That is, it will be assumed that there is no secondary flow within the converging flow field. This is justified by both the stress and velocity measurements shown in Figures 1 and 3.

Now then, using the cylindrical coordinate system, the velocity field is given by

$$V_r = V_r(r,\theta), \qquad V_\theta = V_z = 0 \tag{1}$$

which upon substitution into the continuity equation,

$$\frac{\partial}{\partial r}(rV_r) = 0 \tag{2}$$

gives

$$V_r(r,\theta) = f(\theta)/r, \qquad V_\theta = V_z = 0, \tag{3}$$

in which $f(\theta)$ is an as yet undetermined function depending on $\theta$ only. The function $f(\theta)$ in eq. (3) will be determined, however, when the equations of motion are solved for $V_r(r,\theta)$, subject to boundary conditions specified as

$$(i) \qquad V_r(r,\theta = \pm \alpha) = 0 \tag{4}$$

$$(ii) \qquad \left(\frac{\partial V_r}{\partial \theta}\right)_{\theta=0} = 0. \tag{5}$$

The equations of motion in cylindrical coordinates can be written as

$$-\frac{\partial p}{\partial r} + \frac{1}{r}\frac{\partial}{\partial r}(r\tau_{rr}) + \frac{1}{r}\frac{\partial \tau_{r\theta}}{\partial \theta} - \frac{\tau_{\theta\theta}}{r} = 0 \tag{6}$$

$$-\frac{1}{r}\frac{\partial p}{\partial \theta} + \frac{1}{r^2}\frac{\partial}{\partial r}(r^2\tau_{r\theta}) + \frac{1}{r}\frac{\partial \tau_{\theta\theta}}{\partial \theta} = 0 \tag{7}$$

when the inertia terms involved are neglected.

It now becomes clear that solution of eqs. (6) and (7) with the aid of eqs. (4) and (5) requires relationships between the components of stress and deformation rate. The relationships sought here are very simple for

Newtonian liquids, and this converging flow problem has been solved for that case.[6,7]

It has been established in previous studies[8,9] that the polymer melts employed in the present series of papers exhibit both non-Newtonian viscous and elastic behavior in steady, simple shearing and also Poiseuille flow. For such materials, it is a well-established fact that the stress is a complicated function of the deformation rate, depending not only on the rate of deformation, but also on its time derivatives (acceleration terms). Furthermore, the local stresses depend not only on the local rate of deformation, but also on the previous history of the fluid. In order to treat flow problems associated with converging flow of viscoelastic fluids in general, the authors concur with the remark made by Bogue and Doughty[10] that use of integral constitutive equations would seem to be more appropriate than differential ones. However, *in polymer melt flow*, use of differential constitutive equations would seem to be justifiable on the grounds that the change of deformation rate in the converging flow field may not be so important. This argument is based on the fact that polymer melt flow even in the entrance region is so slow that the melt can be considered as possessing solid-like properties, giving rise to large values of Deborah number.[11,12]

From the slow flow of polymer melts comes the justification of neglecting the inertia terms in eqs. (6) and (7). Under the experimental conditions at which stress and velocity measurements were taken in the present study, Reynolds numbers in the fully developed region (i.e., the downstream end of the slit) lie somewhere between $10^{-3}$ and $10^{-2}$. This range of extremely low values of Reynolds numbers in polymer melt flow gives us a perfect justification for neglecting the inertial effects when solving the equations of motion.

Again, a choice of constitutive equation, even restricted to the differential type, is somewhat arbitrary to the extent that it reasonably describes the experimentally observed rheological behavior, namely, non-Newtonian viscosity and normal stress effect. Considering the nature of the problem in question, the analysis is expected to become quite complicated even with a constitutive equation of simple form.

In the present study, we have chosen a modified second-order fluid model represented as

$$\tau_{ij} = -pg_{ij} + \eta(\mathrm{II})\hat{A}_{ij}^{(1)} + \beta(\mathrm{II})\hat{A}_i^{k(1)}\hat{A}_{kj}^{(1)} + \nu(\mathrm{II})\hat{A}_{ij}^{(2)} \tag{8}$$

where $A_{ij}^{(1)}$ and $A_{ij}^{(2)}$ are defined as

$$A_{ij}^{(1)} = v_{i,j} + v_{j,i} \tag{9}$$

$$A_{ij}^{(2)} = \frac{\partial A_{ij}^{(1)}}{\partial t} + v^m A_{ij,m}^{(1)} + A_{im}^{(1)} v^m{}_{,j} + A_{mj}^{(1)} v^m{}_{,i}. \tag{10}$$

Note in eq. (8) that $\hat{A}_{ij}^{(1)}$ and $\hat{A}_{ij}^{(2)}$ are the physical components of $\hat{A}_{ij}^{(1)}$ and $\hat{A}_{ij}^{(2)}$, respectively, and that the three material constants $\eta$, $\beta$, and $\nu$ are assumed to be functions of the second invariant, II. Equation (8) has been

suggested by White and Metzner[13] and Bogue.[14] In his work, Bogue[14] represented the memory function, appearing in the integral form of the Coleman-Noll second-order fluid model[15] by a discrete-spectrum form and obtained three material constants of the form

$$\eta(\mathrm{II}) = \sum_{i=1}^{N} \frac{G_i\lambda_i}{1 + a|\mathrm{II}|^{1/2}\lambda_i} \tag{11}$$

$$\beta(\mathrm{II}) = \sum_{i=1}^{N} \frac{4G_i\lambda_i^2}{1 + a|\mathrm{II}|^{1/2}\lambda_i)^2} \tag{12}$$

$$-\nu(\mathrm{II}) = \sum_{i=1}^{N} \frac{G_i\lambda_i^2}{(1 + a|\mathrm{II}|^{1/2}\lambda_i)^2}. \tag{13}$$

Because of the complexity of the equations of motion to be solved here, we shall not use eqs. (11) to (13). Instead, we shall use a simple power-law relationship between the material constants and the second invariant. Thus,

$$\eta(\mathrm{II}) = K_1\left[\frac{1}{2}\,\mathrm{II}\right]^{m/2} \tag{14}$$

$$\beta(\mathrm{II}) = K_2\left[\frac{1}{2}\,\mathrm{II}\right]^{P/2} \tag{15}$$

$$-\nu(\mathrm{II}) = K_3\left[\frac{1}{2}\,\mathrm{II}\right]^{q/2} \tag{16}$$

Note that constants $K_1$, $K_2$, $K_3$, $m$, $p$, and $q$ can be determined from the use of experimental data obtained under viscometric flow conditions.

For the velocity field given by eq. (3), one has

$$\hat{\mathbf{A}}^{(1)} = \frac{1}{r^2}\begin{Vmatrix} -2f & f' & 0 \\ f' & 2f & 0 \\ 0 & 0 & 0 \end{Vmatrix} \tag{17}$$

$$\hat{\mathbf{A}}^{(2)} = \frac{1}{r^4}\begin{Vmatrix} 8f^2 & -4ff' & 0 \\ -4ff' & 2f'^2 & 0 \\ 0 & 0 & 0 \end{Vmatrix} \tag{18}$$

and

$$\mathrm{II} = tr\hat{\mathbf{A}}^{(1)^2} = \frac{2}{r^4}(4f^2 + f'^2). \tag{19}$$

Use of eqs. (17) to (19) in eq. (8) gives

$$\tau_{rr} = \frac{-2\eta(\mathrm{II})f}{r^2} + \frac{\beta(\mathrm{II})(4f^2 + f'^2)}{r^4} + \frac{8\nu(\mathrm{II})f^2}{r^4} \tag{20}$$

$$\tau_{\theta\theta} = \frac{2\eta(\mathrm{II})\mathrm{f}}{r^2} + \frac{\beta(\mathrm{II})(4f^2 + f'^2)}{r^4} + \frac{2\nu(\mathrm{II})f'^2}{r^4} \tag{21}$$

$$\tau_{r\theta} = \frac{\eta(\Pi)f'}{r^2} - \frac{4\nu(\Pi)ff'}{r^4} \tag{22}$$

$$\tau_{rr} - \tau_{\theta\theta} = \frac{-4\eta(\Pi)f}{r^2} + \frac{\nu(\Pi)(8f^2 - 2f'^2)}{r^4} \tag{23}$$

in which

$$\eta(\Pi) = \frac{K_1[\Phi]^{m/2}}{r^{2m}} \tag{24}$$

$$\beta(\Pi) = \frac{K_2[\Phi]^{P/2}}{r^{2P}} \tag{25}$$

$$-\nu(\Pi) = \frac{K_3[\Phi]^{q/2}}{r^{2q}} \tag{26}$$

where

$$\Phi = 4f^2 + f'^2. \tag{27}$$

Substitution of eqs. (20) to (22), together with eqs. (24) to (26), into eqs. (6) and (7) will presumably yield an expression which is to be solved for $f(\theta)$. However, one will soon find that, unless a restriction is placed on the indices of power-law equations given by eqs. (14) to (16) such as

$$p = q = m - 1, \tag{28}$$

the system of equations will not be amenable to solution. Now, using the restriction given by eq. (28) and the relationships given by eqs. (20) to (22), the equations of motion, eqs. (6) and (7), become

$$\frac{-\partial p}{\partial r} + \frac{A(\theta)}{r^{2m+3}} + \frac{B(\theta)}{r^{2m+3}} - \frac{C(\theta)}{r^{2m+3}} = 0 \tag{29}$$

$$\frac{-\partial p}{\partial \theta} + \frac{D(\theta)}{r^{2m+2}} + \frac{E(\theta)}{r^{2m+2}} = 0 \tag{30}$$

where

$$A(\theta) = (2m + 1)(2K_1\Phi^{m/2}f - K_2\Phi^{(m+1)/2} + 8K_3\Phi^{(m-1)/2}f^2) \tag{31}$$

$$B(\theta) = K_1\left(\frac{m}{2}\Phi^{(m-2)/2}\Phi'f' + \Phi^{m/2}f''\right) + 4K_3\left(\frac{m-1}{2}\Phi^{(m-3)/2}\Phi'ff' + \Phi^{(m-1)/2}(f'^2 + ff'')\right) \tag{32}$$

$$C(\theta) = 2K_1\Phi^{m/2}f + K_2\Phi^{(m+1)/2} - 2K_3\Phi^{(m-1)/2}f'^2 \tag{33}$$

$$D(\theta) = -2m(K_1\Phi^{m/2}f' + 4K_3\Phi^{(m-1)/2}ff') \tag{34}$$

$$E(\theta) = K_1(m\Phi^{(m-2)/2}\Phi'f + 2\Phi^{m/2}f') + \left(\frac{m+1}{2}\right)K_2\Phi^{(m-1)/2}\Phi' - K_3((m-1)\Phi^{(m-2)/2}\Phi'f'^2 + 4\Phi^{(m-1)/2}f'f'') \tag{35}$$

in which

$$\Phi' = \frac{\mathrm{d}}{d\theta}(4f^2 + f'^2). \tag{36}$$

One can now eliminate the pressure terms from eqs. (29) and (30) by differentiating eq. (29) with respect to $\theta$ and eq. (30) with respect to $r$ and combining the resulting expressions:

$$A'(\theta) + B'(\theta) - C'(\theta) + 2(\mathrm{m} + 1)D(\theta) + 2(m + 1)E(\theta) = 0 \tag{37}$$

where $\mathrm{A}'(\theta)$, $B'(\theta)$, and $C'(\theta)$ are the derivatives of $A(\theta)$, $B(\theta)$, and $C(\theta)$, respectively. It has been demonstrated above that the restriction given by eq. (28) has enabled us to eliminate the dependence of the resulting differential equation, Eq. (37), on the independent variable $r$. Thus, one is left with eq. (37), which relates $f$ as a function of $\theta$ only. Solution of eq. (37) for $f$ and substitution into eqs. (22) and (23) will yield expressions for the shear stress and the normal stress difference as functions of $\theta$ and $r$.

It is now seen that eq. (37) is a third-order, nonlinear ordinary differential equation in $f(\theta)$, which should be solved subject to the boundary conditions

$$\text{(i)} \qquad f(\alpha) = 0 \tag{38}$$

$$\text{(ii)} \qquad f'(0) = 0 \tag{39}$$

$$\text{(iii)} \qquad f(0) = \text{constant.} \tag{40}$$

The first boundary condition implies that the velocity is zero at the walls of the wedge, as seen from eq. (4). The second boundary condition is related to the velocity gradient at the centerline of the wedge. One notes that the maximum velocity will occur along the centerline of the wedge. Therefore, the velocity gradient at this point would be equal to zero. Since, for a fixed volumetric flow rate, the maximum centerline velocity remains a constant, any constant value can be used for $f(0)$. However, $f(0)$ is related to the volumetric flow rate, as will be shown below.

Numerical solution of eq. (37) for $f(\theta)$ would pose no difficulty, although an elaborate algebraic manipulation will be needed to rewrite it, with the aid of eqs. (31) to (36), in a form convenient for computation. In the present study, we have recast eq. (37) into a set of three first-order differential equations, by introducing the transformation

$$\left.\begin{aligned} X_1(\theta) &= f(\theta) \\ X_2(\theta) &= f'(\theta) \\ X_3(\theta) &= f''(\theta) \end{aligned}\right\} \tag{41}$$

which then yields

$$\frac{dX_1(\theta)}{d\theta} = X_2(\theta) \tag{42}$$

$$\frac{dX_2(\theta)}{d\theta} = X_3(\theta) \tag{43}$$

$$\frac{dX_3(\theta)}{d\theta} = g(X_1(\theta),X_2(\theta),X_3(\theta)) \tag{44}$$

where

$$g(X_1,X_2,X_3) = [-2(m+1)D(\theta) - 2(m+1)E(\theta) + C'(\theta) - A'(\theta) - F(\theta)]/G(\theta) \tag{45}$$

in which $F(\theta)$ and $G(\theta)$ are defined as

$$F(\theta) = K_1 m \Phi^{(m-2)/2}\left[\frac{(m-2)}{4}\frac{\Phi'^2 X_2}{\Phi} + \Phi' X_3 + 4X_2^3 + 4X_1X_2X_3 + X_2X_3^2\right] + 4(m-1)K_3\Phi^{(m-3)/2}\left[\frac{(m-3)}{4}\frac{\Phi'^2X_1X_2}{\Phi} + \Phi'(X_2^2 + X_1X_3) + 4X_1X_2^3 + X_2X_3(3\Phi + 4X_1^2 + X_1)\right] \tag{46}$$

$$G(\theta) = K_1\Phi^{m/2}\left(\frac{mX_2^2}{\Phi} + 1\right) + 4K_3\Phi^{(m-1)/2}X_1\left(\frac{(m-1)X_2^2}{\Phi} + 1\right) \tag{47}$$

where

$$\left.\begin{aligned}\Phi &= 4X_1^2 + X_2^2\\ \Phi' &= 8X_1X_2 + 2X_2X_3.\end{aligned}\right\} \tag{48}$$

Appropriate boundary conditions for eqs. (42) to (44) are

$$\text{(i)} \quad X_1(0) = \text{constant} \tag{49}$$

$$\text{(ii)} \quad X_2(0) = 0 \tag{50}$$

$$\text{(iii)} \quad X_1(\alpha) = 0 \tag{51}$$

which follow from eqs. (38) to (40). Note that the initial value of $X_3$, $X_3(0)$ is not known beforehand. However, a computation can be performed by initially assuming $X_3(0)$, and then checking the computed value of $X_1(\alpha)$ against the known value of $X_1(\alpha)$, specified in eq. (51). In other words, a numerical solution of eqs. (42) to (44) can be obtained as an initial-value problem, instead of as a boundary-value problem, using a "shooting" technique suggested by Keller.[16] A predictor-corrector numerical scheme was used to solve the system of differential eqs. (42) to (44). In addition, a Runge-Kutta scheme was used to generate the starting values of the integration.

Once $f(\theta)$ is determined, one can determine the velocity using eq. (3) and the stresses using eqs. (20) to (23). In addition, the volumetric flow

rate can be calculated and compared to experimental values. The volumetric flow rate per unit width of slit is given by

$$\bar{Q} = 2\int_0^\alpha v(r,\theta)rd\theta = 2\int_0^\alpha f(\theta)d\theta. \tag{52}$$

Before we discuss the numerical solution of eqs. (42) to (44), it would be worth considering a few special cases of the modified second-order fluid model given by eq. (8). First, it can be seen that, for *inelastic* power-law fluid, when $K_2 = K_3 = 0$ is substituted into eqs. (31) to (35), one obtains from eq. (37)

$$\frac{d}{d\theta}\left[\Phi^{m/2}\left(4mf + f'' + \frac{m}{2}f\frac{\Phi'}{\Phi}\right)\right] = -2(m+1)\Phi^{m/2}\left[2(1-m)f' + mf\frac{\Phi'}{\Phi}\right] \tag{53}$$

which is identical to the expression obtained by Wissler.[5] Second, for Newtonian fluids, setting $m = 0$ reduces eq. (53) to

$$f''' + 4f' = 0 \tag{54}$$

which also has been discussed in the literature.[6,7]

It has been shown above that the use of the modified second-order fluid model given by eq. (8) can be used to obtain a feasible solution for flow in a converging flow field. However, before these results can be considered, it must be demonstrated that the model does represent a viscoelastic polymeric melt, if not for an entire class, at least for a limited class of materials. This will be shown by substituting the constitutive model into the equation of motion for a simple laminar shearing flow situation. The results of this operation will then be compared with rheogoniometer data obtained for various polymer melts.

## DISCUSSION

### Determination of the Material Constants of the Modified Second-Order Fluid

A truly representative case of simple laminar shearing flow is flow between two infinitely wide parallel plates. This type of flow field can be characterized by

$$v_x = v_x(y), \qquad v_y = v_z = 0 \tag{55}$$

and the velocity gradient is given by

$$v_{x,y} = \dot{\gamma}. \tag{56}$$

Upon substitution of eqs. (55) and (56) into the Eqs. (9) and (10), one obtains the following:

$$\hat{\mathbf{A}}^{(1)} = \begin{Vmatrix} 0 & \dot{\gamma} & 0 \\ \dot{\gamma} & 0 & 0 \\ 0 & 0 & 0 \end{Vmatrix} \tag{57}$$

$$\hat{\mathbf{A}}^{(2)} = \begin{Vmatrix} 0 & 0 & 0 \\ 0 & 2\dot{\gamma}^2 & 0 \\ 0 & 0 & 0 \end{Vmatrix} \tag{58}$$

and the second invariant becomes

$$\text{II} = tr\hat{\mathbf{A}}^{(1)^2} = 2\dot{\gamma}^2. \tag{59}$$

Substitution of eqs. (57) to (59) into the modified second-order model, Eq. (8), along with the restrictions given in eq. (28), yields the following expressions for the shear stress, the first normal stress difference, and the second normal stress difference, respectively:

$$\tau_{xy} = K_1\dot{\gamma}^{m+1} \tag{60}$$

$$\tau_{xx} - \tau_{yy} = 2K_3\dot{\gamma}^{m+1} \tag{61}$$

$$\tau_{yy} - \tau_{zz} = K_2\dot{\gamma}^{m+1} - 2K_3\dot{\gamma}^{m+1}. \tag{62}$$

It now remains to be shown that eqs. (60) to (62) do represent rheological behavior of the polymer melts investigated. Measurements of the viscoelastic properties of the three polymer melts used in the experimental portion of this study were taken by Han et al.[9], using the Han slit/capillary rheometer at high shear rates and the Weissenberg rheogoniometer at low shear rates. The results of their work are shown in Figures 8 and 9. Figure 8 shows plots of shear stress versus shear rate and Figure 9 plots of first normal stress difference versus shear rate. It should be pointed out

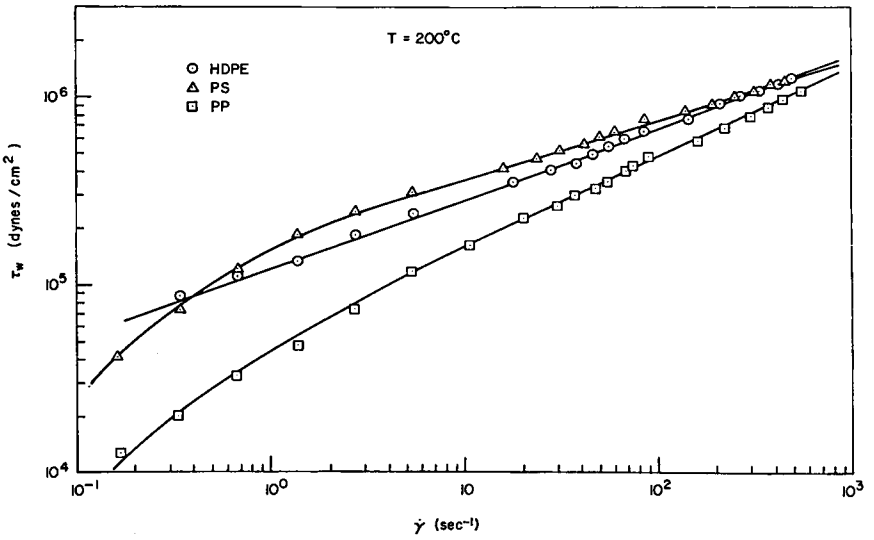


Fig. 8. Plots of shear stress vs. shear rate for three polymer melts investigated.

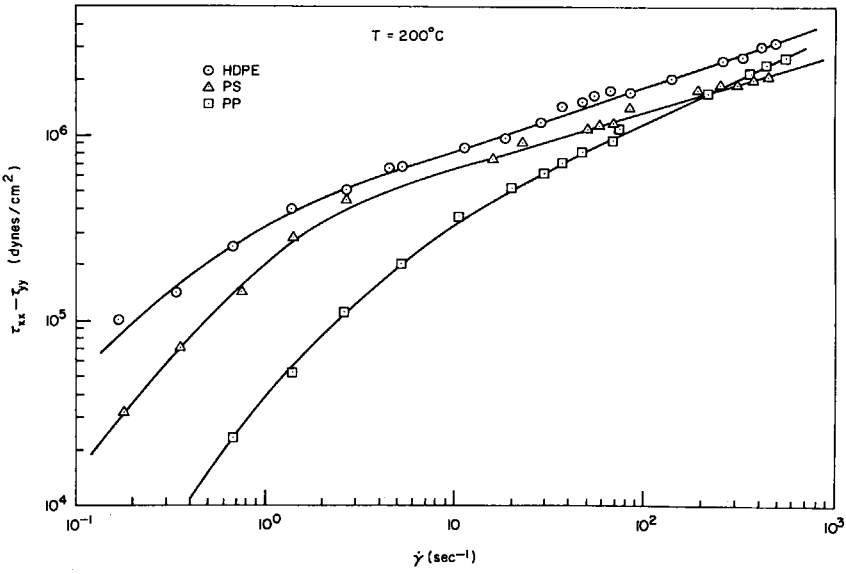


Fig. 9. Plots of normal stress difference vs. shear rate for three polymer melts investigated.

that the first normal stress difference at high shear rates was determined by using the revised theory of Han.[17]

It is seen in Figures 8 and 9 that at high shear rates, say at above 10 sec$^{-1}$, the shear stress and the first normal stress difference both follow a power-law relationship:

$$\tau_{xy} = K\dot{\gamma}^n \tag{63}$$

$$\tau_{xx} - \tau_{yy} = c\dot{\gamma}^d \tag{64}$$

The numerical values of $K$, $n$, $c$, and d obtained from Figures 8 and 9 are given in Table I. It is interesting to note that values of the power-law exponents $n$ and $d$ are very close. In presenting these results, we do *not* wish to claim that all materials should have equal exponents. However, for the materials tested, covering a shear rate range of from, say, 10 to 1000 sec$^{-1}$, this was approximately the situation. While some of the reported

TABLE I
Material Constants of the Polymer Melts Investigated for a Power-Law Fluid

| Material | $K$, $\left(\frac{\text{dynes}}{\text{cm}^2}\ \text{sec}^n\right)$ $\times 15^{-5}$ | $n$ (dimensionless) | $c$, $\left(\frac{\text{dynes}}{\text{cm}^2}\ \text{sec}^n\right)$ $\times 10^{-5}$ | $d$ (dimensionless) |
|---|---|---|---|---|
| Polystyrene | 1.76 | 0.30 | 3.26 | 0.30 |
| Polypropylene | 0.44 | 0.52 | 1.02 | 0.52 |
| High-density polyethylene | 1.18 | 0.37 | 3.55 | 0.35 |

differences may vary as much as 50%, this is a far better approximation than using the Coleman-Noll second-order fluid (15) which predicts:

$$\tau_{xy} = K_1\dot{\gamma} \tag{65}$$

$$\tau_{xx} - \tau_{yy} = 2K_3\dot{\gamma}^2 \tag{66}$$

Therefore, in view of the fact that both the shear stress and the first normal stress difference have approximately equal exponents in the power-law representation given by eqs. (63) and (64), it can be said that eqs. (60) and (61) derived from the modified second-order model, eq. (8), represent flow behavior of the polymer melts investigated in the present study. However, it still remains to be shown that the expression of the second normal stress difference given by eq. (62), too, is reasonable.

During the past decade there have been a number of reports which indicate that the second normal stress difference of viscoelastic fluids is not zero. A few recent papers[18–20] present a summary of the past studies on the subject. At present, a most prevailing evidence, from both the theoretical and experimental points of view, indicates that the second normal stress difference is negative and its magnitude is smaller than the magnitude of the first normal stress difference.[17–20]

Now, one can obtain from eqs. (61) and (62) the ratio of the second normal stress difference to the first:

$$\frac{-(\tau_{yy} - \tau_{zz})}{(\tau_{xx} - \tau_{yy})} = \frac{-(K_2 - 2K_3)}{2K_3} \tag{67}$$

which indicates that the normal stress ratio is constant, independent of shear rate. It should be noted that this conclusion is reached due to the restrictions made in eq. (28). Interestingly enough, however, recent studies[17–20] appear to support eq. (67). For the polymer melts used in the present study, Han[17] reports that $-(\tau_{yy} - \tau_{zz})/(\tau_{xx} - \tau_{yy})$ lies between 0.4 and 0.6, almost independent of shear rate under the conditions investigated. Now then, eq. (67) may be used to determine the material constant $K_2$ from

$$K_2 = 2K_3\,(1 - C_1) \tag{68}$$

in which $C_1$ is a constant, defined by the left-hand side of eq. (67). Using the results of Figures 8 and 9 and the values of $C_1$ reported by Han[17], the constants $m$, $K_1$, $K_2$ and $K_3$ appearing in eqs. (60) to (62) have been determined and they are listed in Table II.

### A Comparison of the Theoretical and the Experimental Results

Figure 10 gives the predicted velocity profiles at $r = 0.1$ cm from the vertex (see Fig. 4), for comparison purposes, of the modified second-order fluid, the power-law fluid, and the Newtonian fluid. Note that all three profiles represent the material flowing with the same volumetric flow rate, $Q = 5.41$ cc/min. One notes that the modified second-order fluid gives a

TABLE II
Material Constants of the Polymer Melts Investigated for a Modified Second-Order Fluid

| Material | $m$ (dimensionless) | $K_1$, $\left(\frac{\text{dynes}}{\text{cm}^2}\ \text{sec}^n\right)$ $\times 10^{-5}$ | $K_2$, $\left(\frac{\text{dynes}}{\text{cm}^2}\ \text{sec}^n\right)$ $\times 10^{-5}$ | $K_3$, $\left(\frac{\text{dynes}}{\text{cm}^2}\ \text{sec}^n\right)$ $\times 10^{-5}$ |
|---|---|---|---|---|
| Polystyrene | −0.69 | 1.73 | 1.77 | 1.64 |
| Polypropylene | −0.48 | 0.45 | 0.46 | 0.52 |
| High-density polyethylene | −0.62 | 1.18 | 2.02 | 1.74 |

flatter velocity profile across the center than the other two fluids, and that it further predicts a lower centerline velocity than either the power-law or the Newtonian fluids. An extensive computation has been carried out to cover a wide range of flow rates, wedge angles, material constants, etc. However, space limitation here does not permit us to present these computed velocity profiles. As noted previously, the boundary condition given in eq. (40) has been determined by the volumetric flow rate. Since various flow rates were tested, the value of $f(0)$ had to be changed. Table III shows how, for a given set of $m$, $K_1$, $K_2$, and $K_3$, the terms $f(0)$, $Q$, and $f''(0)$ vary.

At this point, it is worth taking a close look, once again, at the experimentally determined velocity profiles given in Figure 7 in view of Figure 10. It is seen that the experimental velocity profiles have shapes similar in appearance to those for a Newtonian fluid, and yet the centerline velocity

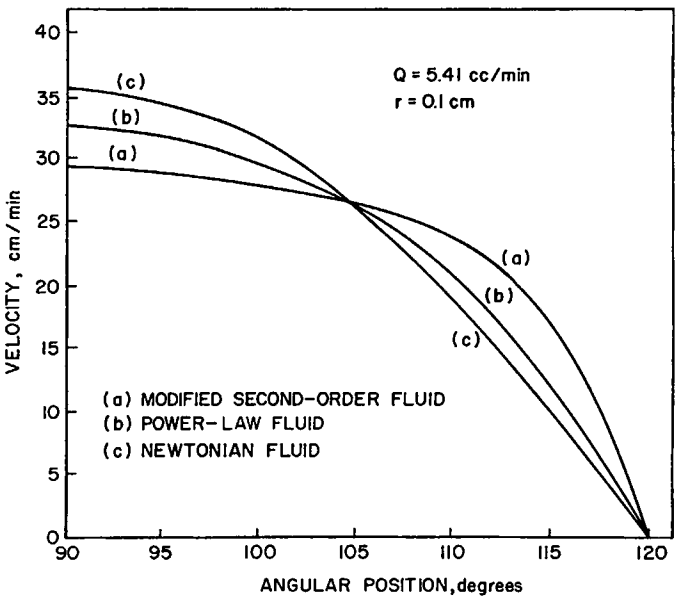


Fig. 10. Theoretically predicted velocity profiles ($Q$ = 5.41 cc/min).

TABLE III
Computed Data for Flow of a Modified Second-Order Fluid into a Converging Channel

| f(0), cm²/sec | $\bar{Q}$, cc/sec/width | $f''(0)$, cm²/sec |
|---|---|---|
| 0.040 | 0.0334 | −0.124 |
| 0.049 | 0.0411 | −0.151 |
| 0.051 | 0.0428 | −0.157 |
| 0.077 | 0.0642 | −0.235 |
| 0.100 | 0.0841 | −0.306 |
| 0.150 | 0.1270 | −0.455 |

of the experimental profile comes closer to what would be predicted for a modified second-order fluid. It can be said that the theoretical analysis presented in this paper predicts velocity profiles which are sensitive to the individual constitutive equations. Also, it can be said from Figure 7 that the agreement between the experimental and theoretical (solid line) results near the centerline is very good. As noted in a previous paper,[2] the scatter of the data away from the centerline is most probably due to the fact that when streaklines were photographed the camera was focused at the centerline. To the best of the authors' knowledge, this is the first

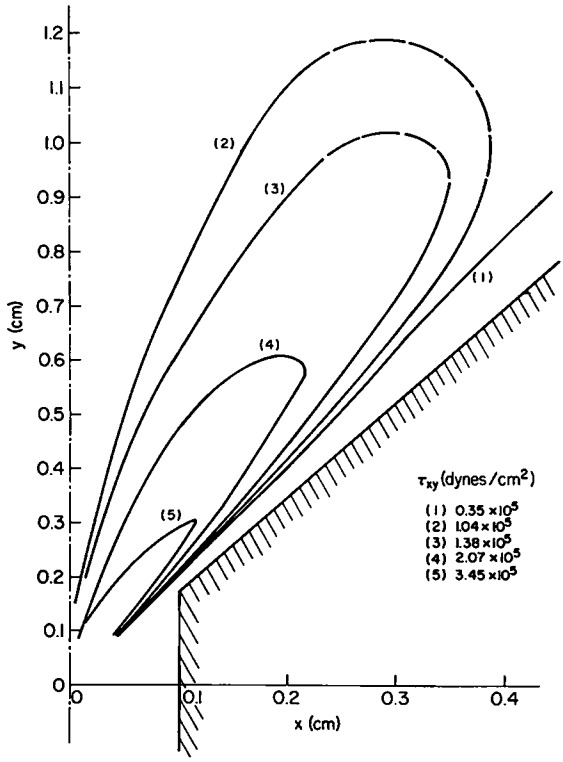


Fig. 11. Theoretically predicted profiles of shear stress for polystyrene using the modified second-order constitutive equation; $Q$ = 5.36 cc/min.

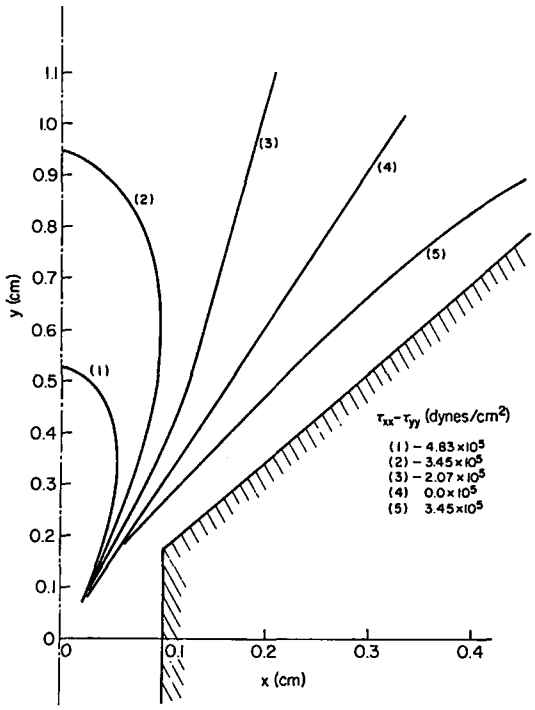


Fig. 12. Theoretically predicted profiles of normal stress difference for polystyrene using the modified second-order constitutive equation; $Q = 5.36$ cc/min.

attempt made at comparing experimentally determined velocity profiles with theoretically predicted ones, in the flow of *polymer melts* through a converging channel.

The numerical results of $f$, $f'$, and $f''$ as a function of $\theta$ can be substituted into eqs. (22) and (23) in order to calculate the shear stress and the normal stress difference. When this is done, one obtains values of the stresses in the cylindrical coordinate system. Since the flow birefringence techniques used in the experimental portion of this investigation utilizes the rectangular coordinate system, a direct comparison of results is not possible, unless one system is transformed into the other. For this reason, the theoretical stresses calculated in the cylindrical coordinate system have been converted into the rectangular coordinate system. This transformation was accomplished with the following set of equations, which were derived by Adams[21]:

$$\tau_{xx} - \tau_{yy} = \left[\frac{(\tau_{rr} - \tau_{\theta\theta}) - 2\tau_{r\theta}\tan 2\theta}{\cos 2\theta[1 + \tan^2 2\theta]}\right] \tag{69}$$

and

$$\tau_{xy} = \frac{-\tau_{r\theta}}{\cos 2\theta} - \frac{\tan 2\theta[(\tau_{rr} - \tau_{\theta\theta}) - 2\tau_{r\theta}\tan 2\theta]}{2\cos 2\theta[1 + \tan^2 2\theta]}. \tag{70}$$

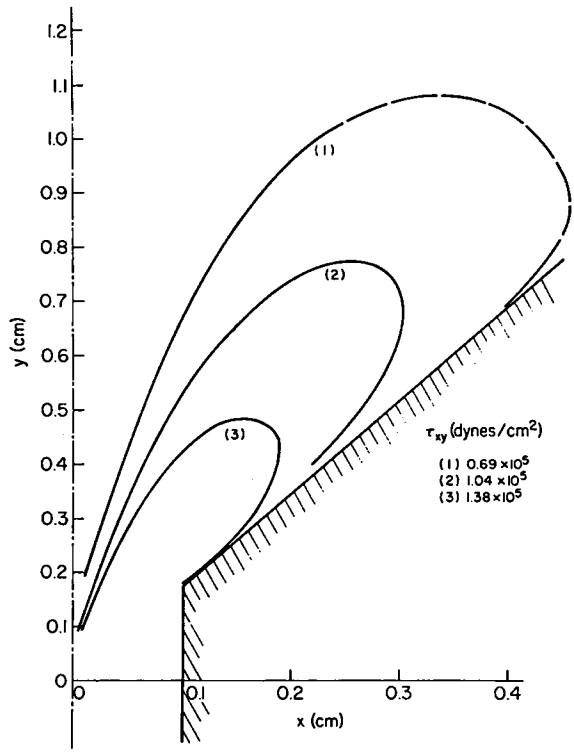


Fig. 13. Theoretically predicted profiles of shear stress for polystyrene using the power-law model; $Q$ = 5.36 cc/min.

Figures 11 and 12 show the theoretically predicted profiles of shear stress and first normal stress difference, using the modified second-order fluid, for polystyrene flowing into the tapered slit die having an entrance angle of 60 degrees.

For comparison purposes, the theoretically predicted shear stress and normal stress profiles are shown in Figures 13 and 14 for a power-law fluid, and in Figures 15 and 16 for a Newtonian fluid. Note that the theoretical profiles in Figure 11 and 16 were obtained for the same volumetric flow rate.

While not much difference is seen between the normal stress difference profiles for different models, except for the actual level of the stress, a major difference is seen in the shear stress profiles. The difference can be seen in how the shear stress profile approaches the wall of the wedge. In the case of the Newtonian fluid representation (see Fig. 15), the curve ends at the wall. However, the curve for the power-law fluid (see Fig. 13) tends to reverse itself as it approaches the walls. The curve for the modified second-order fluid (see Fig. 11) not only reverses itself near the wall, but actually forms a loop in contrast to the other fluids. Also, an extensive computation has been carried out over a wide range of flow rates, wedge angles, and

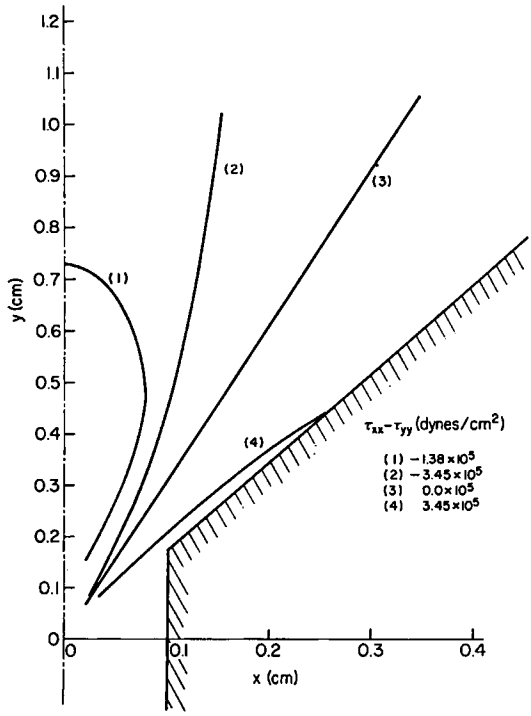


Fig. 14. Theoretically predicted profiles of normal stress difference using the power-law model; $Q$ = 5.36 cc/min.

material constants, etc. However, space limitation here does not permit us to present all those results.

It is now possible to make a comparison between the theoretically determined (Figs. 11 to 16) and the experimentally obtained stress distributions (Figs. 5 and 6). The results of the comparison indicate that the modified second-order model gives a pattern somewhat similar to the experimental profiles. In addition, the stresses are approximately of the same order of magnitude. However, if one compares the Newtonian model shown in Figures 15 and 16 with the experimental profiles, Figures 5 and 6, one obtains a much closer agreement between results. This is not entirely surprising when one computes the shear rate investigated in the slit region under the particular experimental condition being considered, which is about 11 sec$^{-1}$. Although there is no easy way to compute a shear rate for the converging wedge area, one would predict a shear rate of about one or two orders of magnitude smaller than that found in the slit section. As may be seen in Figures 8 and 9, a shear rate of this magnitude in the flow of polystyrene would correspond to either the Newtonian region of the flow curve or at least the transition region. Therefore, it is not surprising to see that the particular experimental data being considered tends to agree more closely with the Newtonian model than with the modified

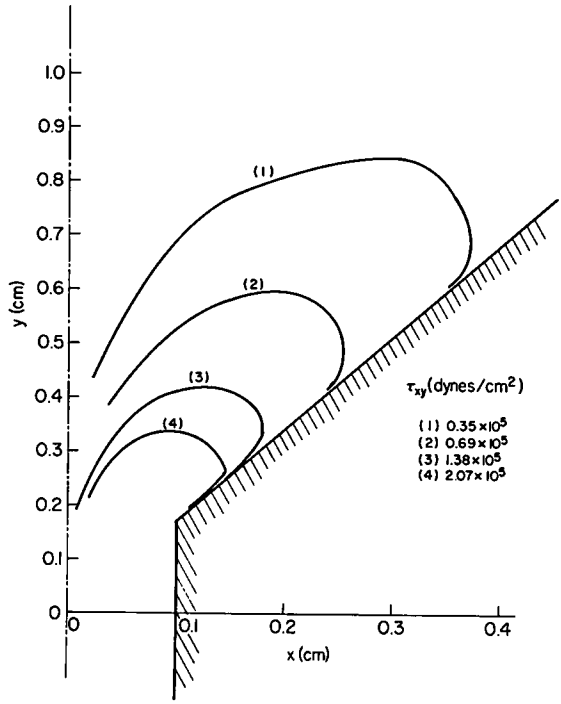


Fig. 15. Theoretically predicted profiles of shear stress for polystyrene using the Newtonian constitutive equation; $Q = 5.36$ cc/min.

second-order model. Due to a limited pumping capacity, very high shear rates were not obtainable. In addition, more important than anything else, as the shear rate was increased for polystyrene, the number of isochromatic fringe patterns increased to such an extent that *identification of the fringe order was not possible.* This, indeed, is a practical limitation of the use of flow birefringence technique.

One should mention at this point that Adams et al.[22] attempted to compare the normal stress difference along the *centerline* predicted by the Coleman-Noll second-order model with their own experimental results obtained with a polymer solution. Later, Fields and Bogue[23] made a similar attempt using a simplified version of the BKZ model[24] in evaluating normal stresses along the centerline of the converging flow field. However, these authors did not make any attempt to compare the stress profiles in the entire converging flow field. That would have required solutions of the equations of motion.

Again, to the best of the authors' knowledge, the study reported above appears to be the first attempt made at comparing the experimentally determined profiles of shear stress and normal stress differences with the theoretically predicted ones, in the flow of polymer melts through a converging channel.

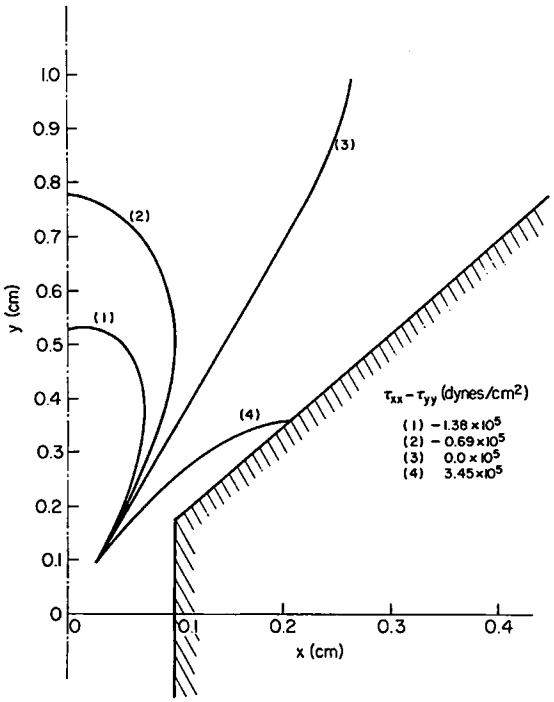


Fig. 16. Theoretically predicted profiles of normal stress difference for polystyrene using the Newtonian constitutive equation; $Q = 5.36$ cc/min.

## CONCLUSIONS

The present study demonstrates once again the usefulness of the experimental techniques of flow birefringence and streak photography for the investigation of polymeric melt flow in a converging channel. The technique of flow birefringence has provided quantitative information of both the shear stress and normal stress difference, and the technique of streak photography has provided information of velocity distributions. It has been found that neither the stress nor velocity measurements indicate any noticeable evidence of circulatory motion when the polymer melts, which are viscoelastic, flow through the converging channel. The apparent absence of circulatory motion, though predicted by earlier theoretical investigations, may be attributed to the very slow motion of polymer melts even in the accelerative flow field concerned. The extremely slow flow of polymer melts (in terms of Reynolds number) has permitted us to make the assumption of creeping flow in carrying the theoretical analysis.

The experimentally obtained profiles of stress and velocity compared favorably with the theoretically predicted ones, which were obtained by numerically solving the equations of motion using a modified second-order constitutive equation. The theoretically predicted profiles of shear stress and normal stress difference are very similar in shape to those obtained by

the flow birefringence experiment. In addition, the values of the stresses are of the same order of magnitude as those found experimentally. The theoretically predicted velocity profiles also are found to be in reasonable agreement with those obtained by the technique of streak photography.

This work was supported in part by the National Science Foundation under Grant GK-23623, for which the authors are grateful.

## References

1. C. D. Han and L. H. Drexler, *J. Appl. Polym. Sci.*, **17**, 2329 (1973).
2. L. H. Drexler and C. D. Han, *J. Appl. Polym. Sci.*, **17**, 2355 (1973).
3. P. N. Kaloni, *J. Phys. Soc.* (Japan), **20**, 132 (1965).
4. P. Schümmer, *Rheol. Acta*, **7**, 271 (1968).
5. E. H. Wissler, *Ind. Eng. Chem., Fundam.*, **10**, 411 (1971).
6. K. Millsaps and K. Pohlhausen, *Aero. Sci.*, **20**, 187 (1953).
7. H. Schlichting, *Boundary Layer Theory*, 4th ed., McGraw-Hill, New York, 1960.
8. C. D. Han, M. Charles, and W. Philippoff, *Trans. Soc. Rheol.*, **14**, 393 (1970).
9. C. D. Han, K. U. Kim, N. Siskovic, and C. R. Huang, *J. Appl. Polym. Sci.*, **17**, 95 (1973).
10. D. C. Bogue and J. O. Doughty, *Ind. Eng. Chem., Fundam.*, **5**, 243 (1966).
11. M. Reiner, *Physics Today*, **17** (No. 1), 62 (1964).
12. A. B. Metzner, J. L. White, and M. M. Denn, *A.I.Ch.E. J.*, **12**, 863 (1966).
13. J. L. White and A. B. Metzner, *A.I.Ch.E. J.*, **11**, 324 (1965).
14. D. C. Bogue, *Ind. Eng. Chem., Fundam.*, **5**, 253 (1966).
15. B. D. Coleman and W. Noll, *Ann. N. Y. Acad. Sci.*, **89**, 672 (1961).
16. H. B. Keller, *Numerical Methods for Two-Point Boundary-Value Problems*, Blaisdell, Waltham, Mass., 1968.
17. C. D. Han, *Trans. Soc. Rheol.*, in press.
18. R. Ginn and A. B. Metzner, *Trans. Soc. Rheol.*, **13**, 429 (1969).
19. O. Olabisi and M. C. Williams, *Trans. Soc. Rheol.*, **16**, 727 (1972).
20. M. J. Miller and E. B. Christiansen, *A.I.Ch.E. J.*, **18**, 600 (1972).
21. E. B. Adams, M.S. Thesis (Ch.E.), University of Tennessee, Knoxville, Tennessee, 1964.
22. E. B. Adams, J. C. Whitehead, and D. C. Bogue, *A.I.Ch.E. J.*, **11**, 1026 (1965).
23. T. R. Fields and D. C. Bogue, *Trans. Soc. Rheol.*, **12**, 39 (1968).
24. B. Bernstein, K. Kearsley, and L. Zapas, *Trans. Soc. Rheol.*, **7**, 391 (1963).

Received October 6, 1972